Materials Science in Semiconductor Processing 131 (2021) 105882

Contents lists available at ScienceDirect

Materials Science in Semiconductor Processing

journal homepage: http://www.elsevier.com/locate/mssp

Analysis of temperature-dependent *I-V* characteristics of the Au/*n*-GaSb Schottky diode

Junho Jang [a,1], Jaeman Song [b,c,1], Seung S. Lee [b], Sangkwon Jeong [b], Bong Jae Lee [b,c,**], Sanghyeon Kim [a,*]

[a] School of Electrical Engineering, Korea Advanced Institute of Science and Technology, Daejeon, 34141, South Korea
[b] Department of Mechanical Engineering, Korea Advanced Institute of Science and Technology, Daejeon, 34141, South Korea
[c] Center for Extreme Thermal Physics and Manufacturing, Korea Advanced Institute of Science and Technology, Daejeon, 34141, South Korea

ARTICLE INFO

Keywords:
GaSb
Schottky diode
Thermionic emission
Tunneling
SRH recombination
Barrier inhomogeneity

ABSTRACT

Gallium antimonide (GaSb) has been widely used for optoelectronic devices in recent years, but the current transport mechanism at the metal-GaSb junction has not yet been clearly identified. In this work, current-voltage (*I-V*) characteristics of Au/*n*-GaSb Schottky diodes were analyzed over a wide temperature range (80–340 K) to investigate their current transport mechanisms. Based on the theory that the total current is described as a contribution of several current mechanisms, the measured *I-V* curves were separated into two components: thermionic emission (TE) current and secondary current. For the TE current, which is the primary current for general Schottky diodes, Schottky diode parameters were extracted and the inhomogeneity of the Schottky barrier was quantified using the temperature dependence of the parameters. For the secondary current, a temperature-dependent predominance between tunneling and Shockley-Read-Hall (SRH) recombination currents was identified by comparing a coefficient of the secondary current with the tunneling coefficient and 2*kT*. We also revealed that other current transport mechanisms such as Auger and radiative recombination, and leakage currents are negligible for the Au/*n*-GaSb Schottky diodes in this work. The methodology suggested in this study can be applied for detailed characterization of various Schottky diodes of which the current transport mechanisms are unidentified.

1. Introduction

Gallium antimonide (GaSb) is a versatile III-V semiconductor for high-speed-optoelectronic devices. The typical GaSb properties of 0.72 eV band-gap energy and hole mobility higher than other III-V semiconductors make this semiconductor suitable for high-speed near-infrared devices. Moreover, GaSb is a great substrate for epitaxial growth because its lattice constant matches those of various ternary and quaternary III-V compounds, such as InGaAsSb and AlGaSb. For these reasons, GaSb based multilayer systems are paid much attention as promising candidates for light-emitting diodes (LED) [1], quantum well laser diodes [2], field-effect transistors [3–5], infrared photodetectors [6,7], multi-layer solar cells [8], and thermophotovoltaic systems [9].

A metal-semiconductor Schottky contact is a basic structure used to realize the aforementioned devices. To form a stable Schottky contact, many studies have been conducted involving surface cleaning and surface passivation methods to treat properly the native oxidation of GaSb surfaces [10–20]. Various metals have also been tried to make Schottky contacts with GaSb: Au [10,12,13,16,17,20–23], Al [14,24,25], Pd [26], and Ni [27–29]. To identify and evaluate the performance of Schottky diodes, analysis of the temperature-dependent diode properties obtained from current-voltage-temperature (*I-V-T*) measurement has commonly been utilized [30–38]. Huang et al. [27] studied characteristics of the Ni/*n*-GaSb Schottky diode using *I-V-T* measurements in the temperature range of 173–373 K. However, the number of temperature points was insufficient to fully describe the temperature-dependent characteristics. In addition, they only considered a thermionic emission (TE) current to extract the Schottky diode properties, without consideration of other current mechanisms.

Schottky diodes are typically analyzed based on TE theory. However,

* Corresponding author.
** Corresponding author. Department of Mechanical Engineering, Korea Advanced Institute of Science and Technology, Daejeon, 34141, South Korea.
E-mail addresses: bongjae.lee@kaist.ac.kr (B.J. Lee), shkim.ee@kaist.ac.kr (S. Kim).
[1] Junho Jang and Jaeman Song contributed equally to this work.

https://doi.org/10.1016/j.mssp.2021.105882
Received 27 January 2021; Received in revised form 6 April 2021; Accepted 11 April 2021
Available online 24 April 2021
1369-8001/

if the doping concentration of the semiconductor is high, the effective mass of the carrier is low, or the temperature of the device is low; the tunneling current becomes the predominant mechanism [39,40]. In the case of GaSb, the effective electron mass is extremely low and the doping concentration of the *n*-type substrate is usually high (around 10^{17} cm^{-3}). This means that the tunneling current should be considered for the *n*-GaSb Schottky diode. Moreover, the Shockley-Read-Hall (SRH) recombination current can also be significant because of defects formed by numerous factors (i.e., defects at the Schottky junction, impurities in the substrate, or oxides formed at the surface). If current mechanisms other than TE cannot be neglected, multiple mechanisms must be reflected to precisely investigate the total current. Donoval et al. [41–43] proposed the multi-current fitting method by assuming that the total current is composed of TE, tunneling, generation-recombination, and leakage currents. They analyzed the forward *I-V* characteristics of Si and InAlN Schottky diodes and showed excellent agreement between measured and fitted curves. However, their fitting procedure was not clearly described even though numerous fitting factors are related to each other.

In this study, *I-V* characteristics of an Au/*n*-GaSb Schottky diode were measured over a wide temperature range of 80–340 K. The *I-V* curves are fitted to an equation for which the sum is of the TE current and of the secondary current composed of tunneling and SRH recombination currents. Furthermore, the temperature dependence of the extracted thermionic emission parameters was explained by the barrier inhomogeneity theory [44]. Tunneling and SRH recombination currents and their parameters were also analyzed using a temperature-dependent secondary current coefficient.

2. Experimental method

One configuration of an Au-GaSb Schottky diode is illustrated in Fig. 1. To fabricate the Au/*n*-GaSb Schottky diode, an *n*-type GaSb wafer with doping concentration of 2×10^{17} cm^{-3} was used as a substrate. At first, a wafer was diced into 6 × 6 mm-square chips. The GaSb chips were degreased in acetone and methanol, and treated in 37% concentrated HCl solution to remove native oxide. After the chips were thoroughly rinsed using IPA, a 150 nm-thick AuGe metal alloy was deposited on the back side of the chips using an electron-beam evaporator. To form an ohmic contact, samples were annealed at 300°C for 4 min in a furnace. A 50 nm-thick Au Schottky electrode was deposited using an electron-beam evaporator on the front side through a 900-μm-diameter patterned shadow mask. To prevent the surface oxidation of GaSb, an SU-8 (Kayaku Advanced Materials, Inc.) photoresist (PR) passivation layer was patterned by photolithography. After that, the Cr/Ag layer was deposited on the PR layer using an electron-beam evaporator to form an electrode connection.

The fabricated Au/*n*-GaSb Schottky diode was loaded on the temperature-controllable Cu stage located in a vacuum chamber. Getting the temperature lower than room temperature was achieved by connecting the Cu stage to a cooling system (Polycold PCC Compact Cooler, Brooks Automation, Inc.). By heating the bottom side of the Cu stage using a ceramic heater (CER-1-01-00540, Watlow Electric Manufacturing Co., Inc.), we obtained a temperature higher than room temperature. While the temperature of the Cu stage was slowly returning to room temperature after being cooled to 84 K or heated to 340 K, *I-V* curves were collected every 10 min by a source meter (2400 SourceMeter, Keithley Instruments, Inc.). The voltage range was from -0.5 to 0.5 V with an interval of 0.005 V. Then, the corresponding temperature was recorded using a Si diode temperature sensor (DT-670, Lake Shore Cryotronics, Inc.).

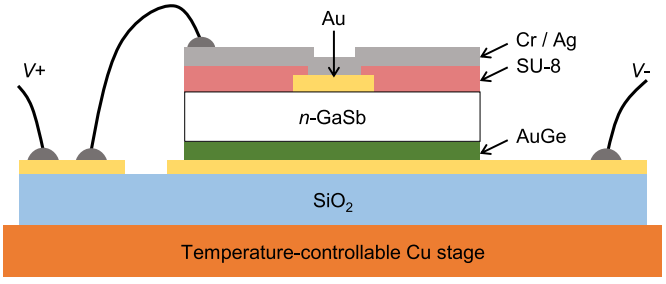

Fig. 1. Schematic diagram of an Au/*n*-GaSb Schottky diode. The diameter and the thickness of an Au Schottky electrode is 900 μm and 50 nm, respectively. The temperature of the Schottky diode is controlled by changing the temperature of the Cu stage which is located in a vacuum chamber.

3. Results and discussion

3.1. Fitting of experimental data

Fig. 2 shows the experimental current density (*J*) and voltage (*V*) characteristics of the Au/*n*-GaSb Schottky diode at several selected temperatures. It was found that both forward and reverse bias currents increase as the temperature rises. We obtained good rectifying behavior with a high on/off current ratio ($>10^3$) at every temperature. Looking at the shape of the forward bias current according to temperature, it can be seen that the slopes of the graphs are irregular, particularly at the lower temperature. From this, it could easily be expected that the total current flowing in the Au/*n*-GaSb Schottky diode is composed of two or more current mechanisms. As reported by Donoval et al. [41–43], the total Schottky diode current can be expressed as the sum of all current components: thermionic emission (J_{TE}), tunneling (J_{TU}), generation-recombination (J_{GR}), and leakage (J_{RL}) currents. With consideration of the effect of the series resistance, they are expressed as [43],

$$J_{tot} = J_{TE} + J_{TU} + J_{GR} + J_{RL} \quad (1)$$

$$J_{TE} = J_{TE(0)}\{\exp[q(V - IR_S)/nkT] - 1\} \quad (2)$$

$$J_{TU} = J_{TU(0)}\{\exp[q(V - IR_S)/E_t] - 1\} \quad (3)$$

$$J_{GR} = J_{GR(0)}\{\exp[q(V - IR_S)/2\ \mathrm{kT}\ ] - 1\} \quad (4)$$

$$J_{RL} = (V - IR_S)/R_L \quad (5)$$

where $J_{TE(0)}$, $J_{TU(0)}$, and $J_{GR(0)}$ are saturation current densities of each current, n is an ideality factor, E_t is a tunneling constant, R_S is a series resistance, and R_L is a resistance corresponding to the leakage current. Although each current component can be obtained by fitting the

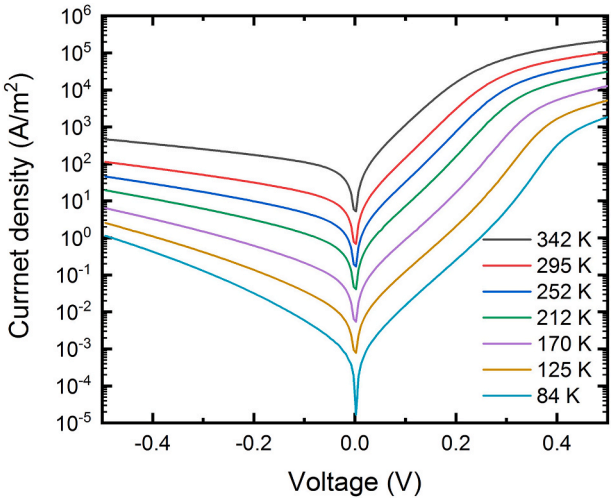

Fig. 2. Experimental current density-voltage characteristics of an Au/*n*-GaSb Schottky diode at several different temperatures.

measured *I-V* curve to Eq. (1), it is difficult to consider all current mechanisms at once because various parameters are related to each other in complicated ways in the total current [see Eqs. (1)–(5)]. Therefore, at first, forward bias currents were fitted under the assumption that the current consists of two current components: TE current and the secondary current (J_{sec}). It was assumed that the secondary current is composed of tunneling current (J_{TU}) and SRH recombination current (J_{SRH}). Other recombination currents including Auger and radiative as well as leakage current will be discussed in Section 3.4. The equation used for fitting is as follows.

$$\begin{aligned} J_{tot} &= J_{TE} + J_{sec} \\ &= J_{TE(0)}\{\exp[q(V - I R_S)/nkT] - 1\} \\ &\quad + J_{sec(0)}\{\exp[q(V - I R_S)/E_{sec}] - 1\} \\ &= J_{TE(0)}\{\exp[q(V - I R_S)/nkT] - 1\} \\ &\quad + J_{TU(0)}\{\exp[q(V - I R_S)/E_t] - 1\} \\ &\quad + J_{SRH(0)}\{\exp[q(V - I R_S)/2kT] - 1\} \end{aligned} \tag{6}$$

Here, we designated $J_{sec(0)}$ and E_{sec} as the saturation current density of the secondary current and a secondary current coefficient, respectively. Measured currents were fitted to Eq. (6) using the MATLAB curve-fitting toolbox.

In Fig. 3, fitted and measured *I-V* curves are described at temperatures of 84, 212, and 342 K. It is confirmed that the sum of J_{TE} and J_{sec} [i.e., Eq. (6)] agree excellently well with the measured current density. As shown in Fig. 3(a), J_{TE} and J_{sec} are clearly distinguished at 84 K. At voltage lower than 0.3 V, the magnitude of J_{sec} substantially exceeds that of J_{TE}. As the temperature increases, J_{TE} accounts for a growing portion of the total current [see Fig. 3(b) and (c)]. These *I-V* characteristics as a function of temperature, are consistent with reports in previous works [41–43].

3.2. Thermionic emission current

Schottky barrier height and ideality factor, which are two significant parameters of Schottky diodes, can be extracted from the thermionic emission current equation [i.e., Eq. (2)]. The saturation current density of thermionic emission current ($J_{TE(0)}$) is expressed as in the following equation.

$$J_{TE(0)} = A^* T^2 \exp\left(-\frac{q\phi_b^j}{kT}\right) \tag{7}$$

In Eq. (7), $A^* = 5.16 \times 10^4$ Am^{-2}K^{-2} is a Richardson constant [27, 40] and ϕ_b^j is the Schottky barrier height. Superscript *j* indicates that the barrier height is obtained from the current-voltage characteristics. After the Schottky barrier height and the ideality factor were obtained over the entire temperature range (80–340 K), the temperature dependence of the two parameters was explained using Werner's barrier inhomogeneity theory [44]. According to this theory, by assuming the Gaussian distribution of the inhomogeneous Schottky barrier height, the Schottky barrier height and the ideality factor are related to the temperature as.

$$\phi_b^j = \overline{\phi}_b - \frac{\sigma_s^2}{2kT/q} \tag{8}$$

$$n^{-1} - 1 = -\rho_2 + \frac{\rho_3}{2kT/q} \tag{9}$$

where $\overline{\phi}_b$ is an actual mean barrier height, σ_s is a standard deviation of barrier height, and ρ_2 and ρ_3 are coefficients proportional to the voltage dependence of ϕ_b^j and σ_s, respectively.

Fig. 4 shows extraction results of ϕ_b^j and $n^{-1} - 1$ with respect to $1/T$. As shown in both Fig. 4(a) and (b), given that the three last points from the lowest temperature clearly deviated from linearity, they were excluded from the linear fitting. Because the *n*-GaSb substrate degenerates as the temperature decreases, such deviation could occur. Because the equation of thermionic emission current [Eq. (2)] was derived based on the assumption of a non-degenerate semiconductor, the degenerate effects could lead to overestimation of the barrier height

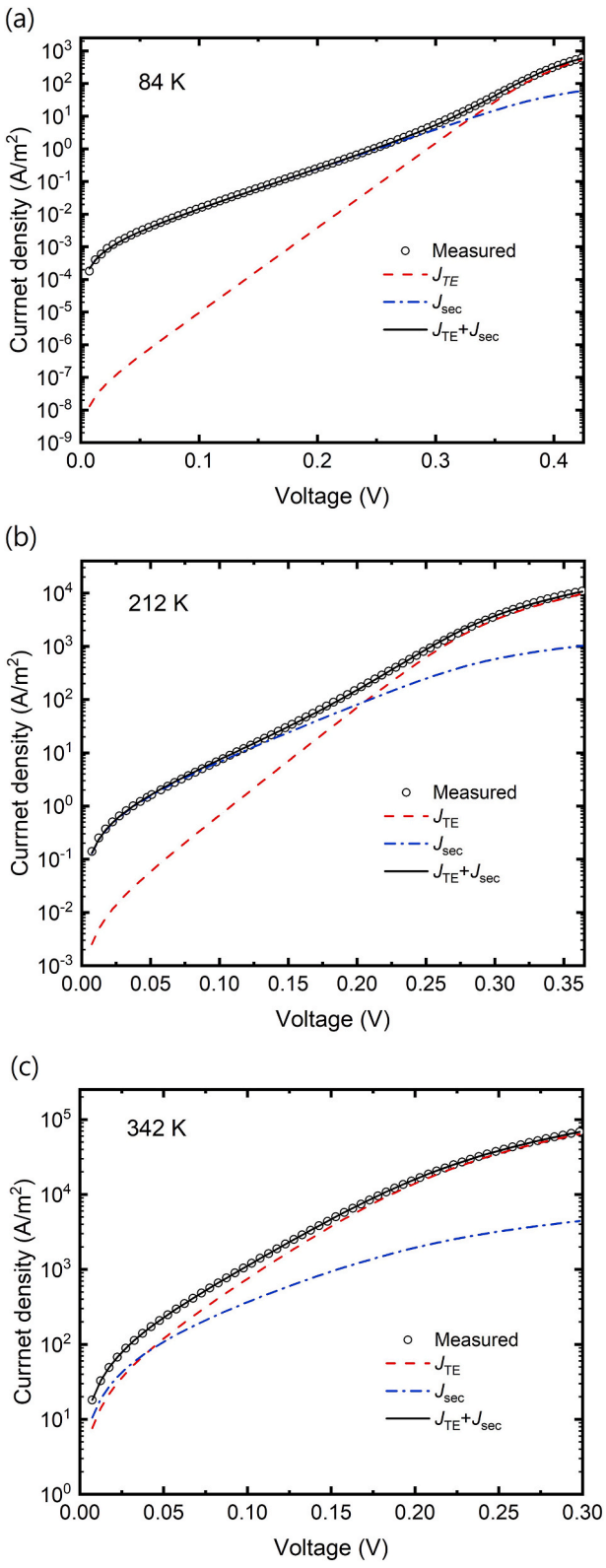

Fig. 3. Fitting results of the forward *I-V* characteristics at (a) 84 K, (b) 212 K, (c) 342 K. A sum of the TE current and the secondary current well matches with the measured current.

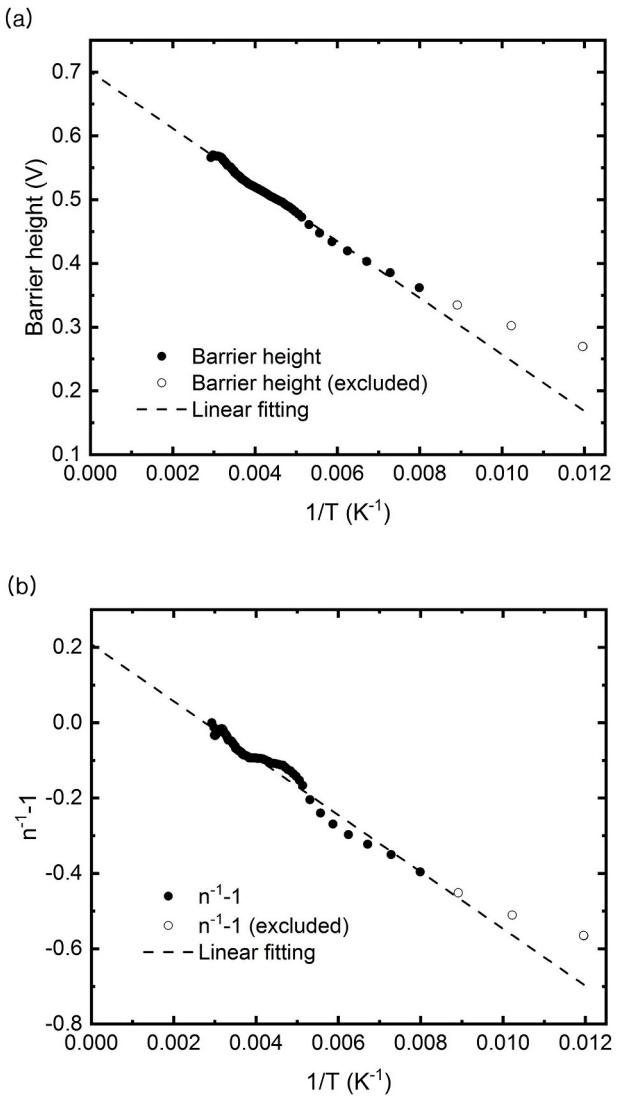

Fig. 4. The temperature-dependent diode properties of the Au/*n*-GaSb Schottky diode following Werner's barrier inhomogeneity theory [44]. (a) Barrier height and (b) $n^{-1}-1$ respect to $1/T$ are plotted. Both (a) and (b) graphs show linear relation with $1/T$ excluding the three lowest temperatures.

and underestimation of the ideality factor compared to the actual values. The barrier heights and ideality factors fit well with Werner's equation, except for the low-temperature points in Fig. 4. The 0.70 V of ϕ_b and 0.087 V of σ_s were obtained from linear fitting of the ϕ_b^j - $1/T$ plot shown in Fig. 4(a). These values are close to those reported by Huang et al. [27]. Considering the band-gap energy of GaSb, the Fermi-level is located near the valence band edge. The ρ_2 and ρ_3 values obtained were -0.2083 and -0.0130 from the $n^{-1}-1$ versus $1/T$ plot shown in Fig. 4 (b) and they are consistent with previous studies on Schottky diodes [44].

3.3. Tunneling and SRH recombination currents

According to Eq. (6), the secondary current is a composite result of the tunneling and the SRH recombination currents. Because the properties of a semiconductor are a function of temperature, the contribution of the two currents to J_{sec} will be clearly distinguished at quite low or high temperatures. In Fig. 5, the magnitude of E_{sec}, which could be a criterion for the predominance of either the tunneling current or the SRH recombination current by temperature, is described. It is clearly

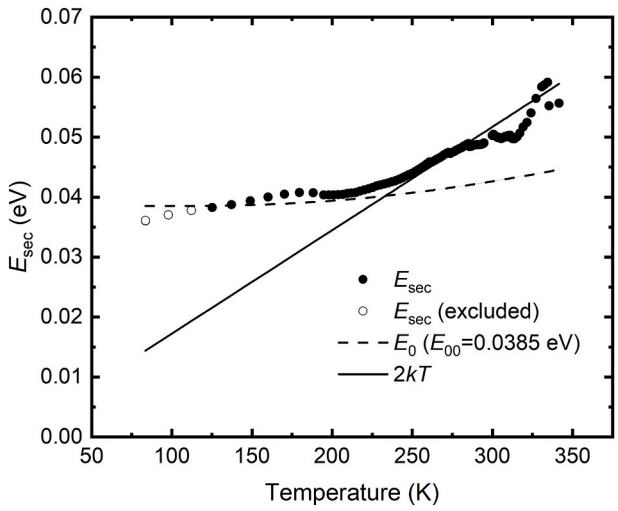

Fig. 5. The secondary current coefficient as a function of temperature. They are compared with the thermionic field emission tunneling coefficient E_0 when E_{00} = 0.0385 eV and 2kT.

shown that E_{sec} follows the 2kT guideline, which is the current coefficient for the SRH recombination current at temperatures above 240 K.

However, E_{sec} and the 2kT guideline do not match at temperatures below 240 K, in which case it could be expected that E_{sec} would follow the tunneling current coefficient better. If the tunneling constant has an order similar to the value of kT ($0.1kT < E_t < 10kT$) [39], thermionic field emission would be a predominant tunneling mechanism. Because the obtained E_{sec} is located in this range, the thermionic field emission theory was employed to analyze the tunneling current. The thermionic field emission tunneling coefficient.

E_0 is expressed as [39,45],

$$E_0 = E_{00}\coth\left(\frac{E_{00}}{kT}\right) \tag{10}$$

where E_{00} is the energy constant of tunneling. It depends on the material properties and the doping concentration of a semiconductor. As the effect of the degenerated semiconductor is considered in the analysis of J_{TE} in Section 3.2, we excluded the lowest three temperature points for the investigation of E_{sec}. As shown in Fig. 5, we can see a good agreement between E_0 and E_{sec} in the low-temperature range when E_{00}=0.0385 eV. Accordingly, it can be supposed that the SRH recombination current is dominant when the temperature is higher than 240 K, and the effect of the tunneling current starts to increase as the temperature decreases.

In Fig. 6, *I-V* curves at 149 and 342 K were again fitted to an equation composed of TE, TU, and SRH recombination currents which is the last term of Eq. (6). The sum of the three current components matched perfectly the measured values. Moreover, the temperature-dependent relative magnitudes of J_{TU} and J_{SRH} correspond with the prediction from E_{sec}. Therefore, it was confirmed that E_{sec} could be used as a criterion for quantifying the contribution of tunneling and SRH recombination to the total current.

SRH recombination occurs due to defects and impurities in a bulk semiconductor or on a semiconductor surface. The equation of the SRH recombination current can be simplified as [40],

$$J_{SRH} \approx \frac{qW_D n_i}{2\tau}\left[\exp\left(\frac{qV}{2kT}\right)-1\right] \tag{11}$$

where W_D is the width of the depletion region, n_i is an intrinsic carrier concentration, and τ is a SRH recombination lifetime. The SRH recombination current is proportional to n_i, which is known as a strongly temperature-dependent property [46]. Because n_i is almost zero at the low temperature, the SRH recombination current can contribute largely

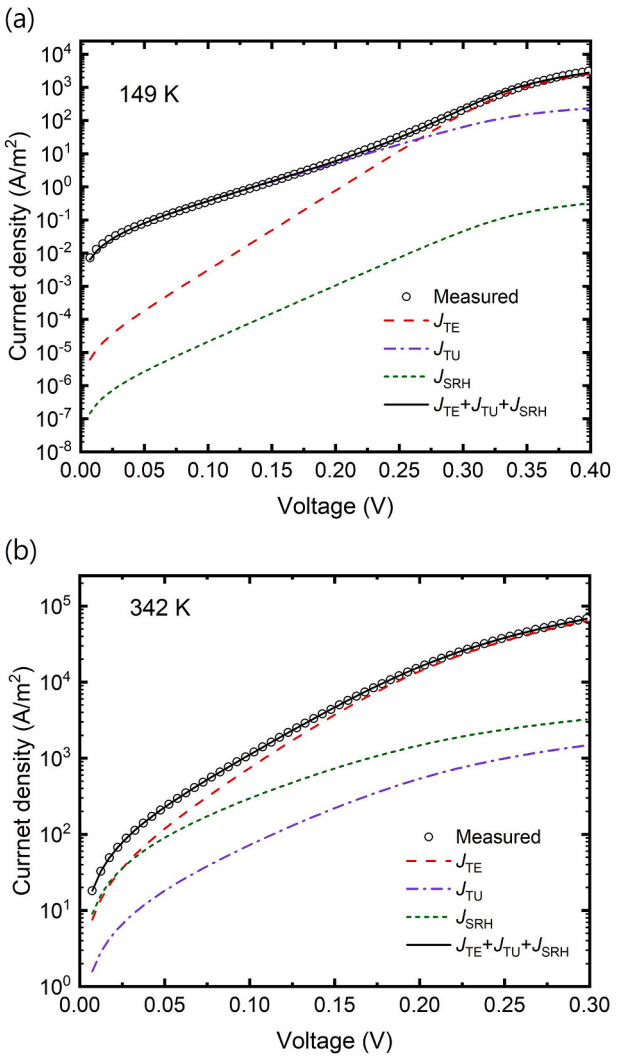

Fig. 6. Fitting results of the forward *I-V* characteristics at (a) 149 K and (b) 342 K including thermionic emission, tunneling, and SRH recombination currents.

to the total current only at the higher temperature. By using Eq. (11), we obtained τ of about 1 ns at 342 K.

3.4. Other current components

When the leakage current, J_{RL} is included in Eq. (6) for fitting to the measurement, J_{RL} is a marginal component compared to J_{TE} and J_{sec}, as shown in Fig. 7. The obtained resistance corresponding to J_{RL} is R_L = 1980 Ωm^2 at 212 K, indicating that J_{RL} can be neglected to analyze J_{TE} and J_{sec}. The leakage current mainly flows through the surface-leakage path; accordingly, the surface-leakage current is proportional to the perimeter of the electrode. Because the Schottky diode used in this study was fabricated with a large diameter (i.e., 900 μm), the perimeter of the electrode is relatively small compared to its area. Thus, the leakage current becomes a negligible component.

Although the Auger recombination current, J_a and the radiative recombination current, J_{rad} are generally considered for a direct band-gap semiconductors like GaSb, these components are not included in the secondary current. Auger and radiative recombination rates are expressed as $R_a = C(n^2p + np^2)$ and $R_{rad} = \beta np$, respectively. For GaSb, the radiative recombination coefficient, β is known to be approximately 10^{-10} cm^3/s [46] and the Auger recombination coefficient, C is known to be approximately 10^{-29} cm^6/s at room temperature [47], where n and p are the carrier concentrations of electrons and holes. Recombination

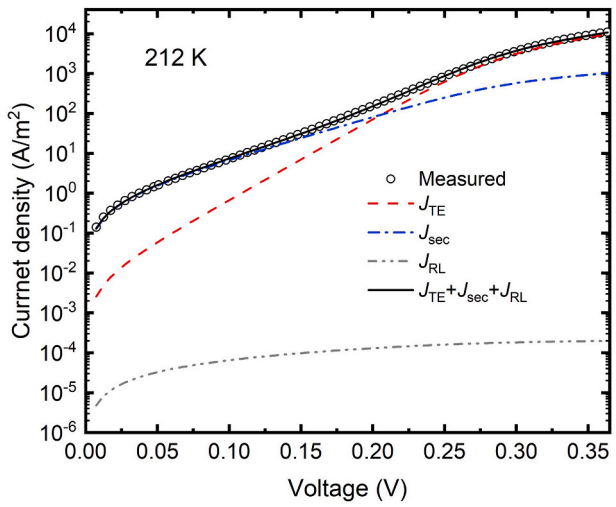

Fig. 7. Fitting results of the forward *I-V* characteristics at 212 K including the leakage current.

rates R_a and R_{rad} over the depletion region. Fig. 8 shows a comparison among the measured current and three recombination currents (i.e., SRH, Auger, and radiative) at room temperature. Here, J_a and J_{rad} are almost negligible compared to J_{SRH}. Unless β and C significantly increase at low or high temperature, Auger and radiative recombination currents will be negligible over the entire temperature range.

4. Conclusions

In this study, the temperature-dependent *I-V* characteristics of the Au/*n*-GaSb Schottky diodes were explored. The *I-V* curves of the diodes were measured over a wide temperature range (80–340 K) and the results were fitted by considering two current components: the thermionic emission current and the secondary current which is composed of the tunneling and SRH recombination currents. The measured *I-V* curves perfectly agree with the sum of the thermionic emission current and the secondary current over the entire temperature range. Thermionic emission parameters, such as the Schottky barrier height and ideality factor, were extracted from the thermionic emission current and the temperature dependence of the parameters was explained using the barrier inhomogeneity theory. Coefficients of the secondary current were compared with a tunneling constant of thermionic field emission

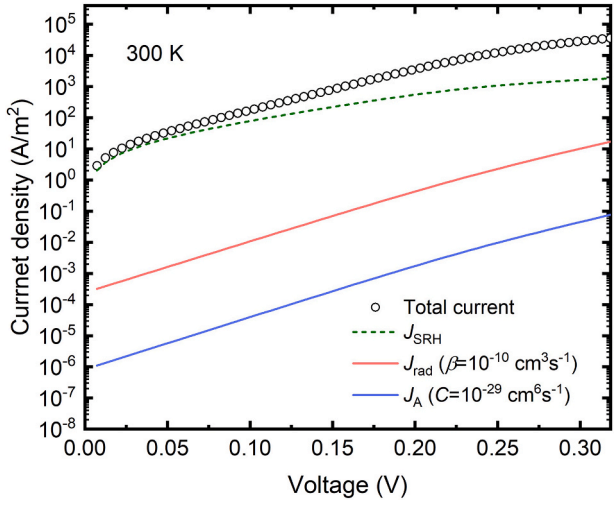

Fig. 8. Comparison of the measured current and calculated radiative and Auger recombination currents at 300 K.

and 2*kT*, corresponding to the coefficient of the SRH recombination current. It was shown that the secondary current is almost governed by the tunneling current at low temperature and the SRH recombination current starts to exert grater effect at temperatures higher than 240 K. Through analysis of the Au/*n*-GaSb Schottky diodes based on Donoval's multi-current fitting method [41–43] and Werner's barrier inhomogeneity theory [44], the current transport mechanism of the GaSb Schottky diodes was more precisely investigated than in previous studies. We expect that the methodology proposed in this study will promote the detailed characterization of various Schottky diodes of which the current mechanisms are unidentified.

CRediT authorship contribution statement

Junho Jang: Conceptualization, Methodology, Data curation, Formal analysis, Writing – original draft. **Jaeman Song:** Conceptualization, Methodology, Data curation, Validation, Writing – review & editing. **Seung S. Lee:** Supervision, Funding acquisition. **Sangkwon Jeong:** Resources. **Bong Jae Lee:** Supervision, Project administration, Funding acquisition. **Sanghyeon Kim:** Supervision, Writing – review & editing, Funding acquisition.

Declaration of competing interest

The authors declare that they have no known competing financial interests or personal relationships that could have appeared to influence the work reported in this paper.

Acknowledgements

This work was supported by National Research Foundation of Korea (NRF-2019R1A2C2003605, NRF-2020R1A4 A4078930, and NRF-2019M1A2A2067928), and by National Nanofab Center (NNFC) OI project.

References

[1] S.-Y. Lin, C.-C. Tseng, W.-H. Lin, S.-C. Mai, S.-Y. Wu, S.-H. Chen, J.-I. Chyi, Room–temperature operation type–II GaSb/GaAs quantum–dot infrared light–emitting diode, Appl. Phys. Lett. 96 (12) (2010), 123503.
[2] O. Delorme, L. Cerutti, E. Luna, G. Narcy, A. Trampert, E. Tournié, J.-B. Rodriguez, GaSbBi/GaSb quantum well laser diodes, Appl. Phys. Lett. 110 (22) (2017), 222106.
[3] E. Memisevic, M. Hellenbrand, E. Lind, A.R. Persson, S. Sant, A. Schenk, J. Svensson, R. Wallenberg, L.-E. Wernersson, Indi- vidual defects in InAs/InGaAsSb/GaSb nanowire tunnel field–effect transistors operating below 60 mv/decade, Nano Lett. 17 (7) (2017) 4373–4380.
[4] S.H. Kim, I.P. Roh, J.H. Han, D.-M. Geum, S.K. Kim, S.S. Kang, H.-K. Kang, W. C. Lee, S.K. Kim, D.K. Hwang, Y.H. Song, J.D. Song, High hole mobility and low leakage thin-body (In)GaSb p-MOSFETs grown on high-bandgap AlGaSb, IEEE J. Electron. Dev. Soc. 9 (2020) 42–48.
[5] W. Lu, I.P. Roh, D.-M. Geum, S.-H. Kim, J.D. Song, L. Kong, J.A. del Alamo, 10-nm fin-width InGaSb p-channel self-aligned Fin- FETs using antimonide-compatible digital etch, in: 2017 IEEE Inter- National Electron Devices Meeting (IEDM), IEEE, 2017, 17–7.
[6] A. Haddadi, R. Chevallier, A. Dehzangi, M. Razeghi, Ex- tended short–wavelength infrared nBn photodetectors based on type– II InAs/AlSb/GaSb superlattices with an AlAsSb/GaSb superlattice barrier, Appl. Phys. Lett. 110 (10) (2017), 101104.
[7] J. Sun, M. Peng, Y. Zhang, L. Zhang, R. Peng, C. Miao, D. Liu, M. Han, R. Feng, Y. Ma, Y. Dai, L. He, C. Shan, A. Pan, W. Hu, Z. Yang, Ultrahigh hole mobility of Sn–catalyzed GaSb nanowires for high speed infrared photodetectors, Nano Lett. 19 (9) (2019) 5920–5929.
[8] M.P. Lumb, S. Mack, K.J. Schmieder, M. González, M.F. Ben- nett, D. Scheiman, M. Meitl, B. Fisher, S. Burroughs, K.-T. Lee, J.A. Rogers, R.J. Walters, GaSb–based solar cells for full solar spec- trum energy harvesting, Adv. Energy Mater. 7 (20) (2017), 1700345.
[9] B.-C. Juang, R.B. Laghumavarapu, B.J. Foggo, P.J. Simmonds, A. Lin, B. Liang, D. L. Huffaker, GaSb thermophotovoltaic cells grown on GaAs by molecular beam epitaxy using interfacial misfit arrays, Appl. Phys. Lett. 106 (11) (2015), 111101.
[10] P. Barman, U.N. Roy, S. Basu, Improved junction properties of Au–*n*–GaSb Schottky diodes after chemical modification of GaSb surfaces, Mater. Lett. 10 (4–5) (1990) 203–206.
[11] P.S. Dutta, K.S. Sangunni, H.L. Bhat, V. Kumar, Sulphur passivation of gallium antimonide surfaces, Appl. Phys. Lett. 65 (13) (1994) 1695–1697.
[12] M. Pérotin, P. Coudray, L. Gouskov, H. Luquet, C. Llinarés, J.J. Bon- net, L. Soonckindt, B. Lambert, Passivation of GaSb by sulfur treatment, J. Electron. Mater. 23 (1) (1994) 7–12.
[13] P.S. Dutta, K.S.R. Koteswara Rao, H.L. Bhat, V. Kumar, Effect of ruthenium passivation on the optical and electrical properties of gallium antimonide, J. Appl. Phys. 77 (9) (1995) 4825–4827.
[14] G. Eftekhari, Effects of sulfur passivation of GaSb on the thermal stability of Al/n–GaSb contacts, Jpn. J. Appl. Phys. 35 (2A) (1996) 564–567.
[15] Z.Y. Liu, B. Hawkins, T.F. Kuech, Chemical and structural characterization of GaSb (100) surfaces treated by HCl–based solu- tions and annealed in vacuum, J. Vac. Sci. Technol. B 21 (1) (2003) 71–77.
[16] Z.Y. Liu, D.A. Saulys, T.F. Kuech, Improved characteristics for Au/n–GaSb Schottky contacts through the use of a nonaqueous sulfide–based passivation, Appl. Phys. Lett. 85 (19) (2004) 4391–4393.
[17] D.M. Murape, N. Eassa, J.H. Neethling, R. Betz, E. Coetsee, H.C. Swart, J.R. Botha, A. Venter, Treatment for GaSb surfaces using a sulphur blended $(NH_4)_2S$/$(NH_4)_2SO_4$ solution, Appl. Surf. Sci. 258 (18) (2012) 6753–6758.
[18] M.V. Lebedev, E.V. Kunitsyna, W. Calvet, T. Mayer, W. Jaegermann, Sulfur passivation of GaSb (100) surfaces: compari- son of aqueous and alcoholic sulfide solutions using synchrotron radi- ation photoemission spectroscopy, J. Phys. Chem. C 117 (31) (2013) 15996–16004.
[19] L. Zhao, Z. Tan, R. Bai, N. Cui, J. Wang, J. Xu, Effects of sulfur passivation on GaSb Metal–Oxide–Semiconductor capacitors with neutralized and unneutralized $(NH_4)_2S$ solutions of varied con- centrations, APEX 6 (5) (2013), 056502.
[20] D. Tao, Y. Cheng, J. Liu, J. Su, T. Liu, F. Yang, F. Wang, K. Cao, Z. Dong, Y. Zhao, Improved surface and electrical properties of passivated GaSb with less alkaline sulfide solution, Mater. Sci. Semicond. Process. 40 (2015) 685–689.
[21] Y. Nagao, T. Hariu, Y. Shibata, GaSb Schottky diodes for infrared detectors, IEEE Trans. Electron. Dev. 28 (4) (1981) 407–411.
[22] B. Rotelli, L. Tarricone, E. Gombia, R. Mosca, M. Perotin, Photoelectric properties of GaSb Schottky diodes, J. Appl. Phys. 81 (4) (1997) 1813–1819.
[23] C.-L. Lin, Y.-K. Su, J.-R. Chang, S.-M. Chen, W.-L. Li, D.-H. Jaw, Temperature dependence of barrier height and energy bandgap in Au/*n*–GaSb Schottky diode, Jpn. J. Appl. Phys. 39 (5A) (2000) L400–L401.
[24] W. Oueini, M. Rouanet, J. Bonnet, Formation of the Al–GaSb (110), Interf. Surf. Sci. 409 (3) (1998) 445–451.
[25] A. Subekti, T.L. Tansley, E.M. Goldys, Tunneling transport in Al–*n*–GaSb Schottky diodes, IEEE Trans. Electron. Dev. 45 (10) (1998) 2247–2248.
[26] Y.K. Su, N.Y. Li, F.S. Juang, S.C. Wu, The effect of annealing temperature on electrical properties of Pd/*n*–GaSb Schottky contacts, J. Appl. Phys. 68 (2) (1990) 646–648.
[27] W.-C. Huang, T.-C. Lin, C.-T. Horng, Y.-H. Li, The electrical characteristics of Ni/n–GaSb Schottky diode, Mater. Sci. Semicond. Process. 16 (2) (2013) 418–423.
[28] K. Nishi, M. Yokoyama, S.H. Kim, H. Yokoyama, M. Takenaka, S. Takagi, Study on electrical properties of metal/GaSb junctions us- ing metal-GaSb alloys, J. Appl. Phys. 115 (3) (2014), 034515.
[29] C.B. Zota, S.-H. Kim, M. Yokoyama, M. Takenaka, S. Takagi, Characterization of Ni-GaSb alloys formed by direct reaction of Ni with GaSb, APEX 5 (7) (2012), 071201.
[30] A. Gümüş, A. Türüt, N. Yalçin, Temperature dependent bar- rier characteristics of CrNiCo alloy Schottky contacts on n–type molecular–beam epitaxy GaAs, J. Appl. Phys. 91 (1) (2002) 245–250.
[31] S. Kumar, Y.S. Katharria, S. Kumar, D. Kanjilal, Temperature– dependence of barrier height of swift heavy ion irradiated Au/n–Si Schottky structure, Solid State Electron. 50 (11–12) (2006) 1835–1837.
[32] W. Mtangi, F.D. Auret, C. Nyamhere, P.J.J. Van Rensburg, M. Diale, A. Chawanda, Analysis of temperature dependent I–V measure- ments on Pd/ZnO Schottky barrier diodes and the determination of the Richardson constant, Physica B 404 (8–11) (2009) 1092–1096.
[33] N. Yıldırım, K. Ejderha, A. Turut, On temperature–dependent experimental I–V and C–V data of Ni/n–GaN Schottky contacts, J. Appl. Phys. 108 (11) (2010), 114506.
[34] Ö.F. Yüksel, M. Kuş, N. Şimşir, H. Şafak, M. Şahin, E. Yenel, A detailed analysis of current–voltage characteristics of Au/perylene– monoimide/n–Si Schottky barrier diodes over a wide temperature range, J. Appl. Phys. 110 (2) (2011), 024507.
[35] D. Korucu, T.S. Mammadov, Temperature–dependent current– conduction mechanisms in Au/n–InP Schottky barrier diodes (SBDs), J. Optoelectron. Adv. Mater. 14 (1) (2012) 41.
[36] D. Korucu, A. Turut, H. Efeoglu, Temperature dependent I–V characteristics of an Au/n–GaAs Schottky diode analyzed using Tung's model, Physica B 414 (2013) 35–41.
[37] K. Zeghdar, L. Dehimi, A. Saadoune, N. Sengouga, Inhomoge- neous barrier height effect on the current–voltage characteristics of an Au/n–InP Schottky diode, J. Semiconduct. 36 (12) (2015), 124002.
[38] S. Mahato, D. Biswas, L.G. Gerling, C. Voz, J. Puigdollers, Analysis of temperature dependent current–voltage and capacitance– voltage characteristics of an Au/V2O5/n–Si Schottky diode, AIP Adv. 7 (8) (2017), 085313.
[39] C.R. Crowell, V.L. Rideout, Normalized thermionic–field (TF) emission in metal–semiconductor (Schottky) barriers, Solid St. Electron. 12 (2) (1969) 89–105.
[40] S.M. Sze, K.K. Ng, Physics of Semiconductor Devices, John Wiley & Sons, 2006.
[41] D. Donoval, M. Barus, M. Zdimal, Analysis of I–V measurements on PtSi–Si Schottky structures in a wide temperature range, Solid State Electron. 34 (12) (1991) 1365–1373.
[42] D. Donoval, A. Chvála, R. Šramatý, J. Kováš, J.-F. Carlin, N. Grand- jean, G. Pozzovivo, J. Kuzmík, D. Pogany, G. Strasser, P. Kor- doš, Current transport and barrier height evaluation in Ni/InAlN/GaN Schottky diodes, Appl. Phys. Lett. 96 (22) (2010), 223501.

[43] D. Donoval, A. Chvála, R. Šramatý, J. Kováš, E. Morvan, Ch Dua, M.A. DiForte-Poisson, P. Kordoš, Transport properties and barrier height evaluation in Ni/InAlN/GaN Schottky diodes, J. Appl. Phys. 109 (6) (2011), 063711.
[44] J.H. Werner, H.H. Güttler, Barrier inhomogeneities at Schottky contacts, J. Appl. Phys. 69 (3) (1991) 1522–1533.
[45] F.A. Padovani, R. Stratton, Field and thermionic–field emission in Schottky barriers, Solid State Electron. 9 (7) (1966) 695–707.
[46] M. Levinshtein, Handbook Series on Semiconductor Parameters, vol. 1, World Scientific, 1997.
[47] M. Takeshima, Auger recombination in InAs, GaSb, InP, and GaAs, J. Appl. Phys. 43 (10) (1972) 4114–4119.